

Kantartzis, P., Abdi, M. & Liatsis, P. (2013). Stimulation and measurement patterns versus prior information for fast 3D EIT: A breast screening case study. *Signal Processing*, 93(10), pp. 2838-2850. doi: 10.1016/j.sigpro.2012.06.027



**CITY UNIVERSITY
LONDON**

[City Research Online](#)

Original citation: Kantartzis, P., Abdi, M. & Liatsis, P. (2013). Stimulation and measurement patterns versus prior information for fast 3D EIT: A breast screening case study. *Signal Processing*, 93(10), pp. 2838-2850. doi: 10.1016/j.sigpro.2012.06.027

Permanent City Research Online URL: <http://openaccess.city.ac.uk/7741/>

Copyright & reuse

City University London has developed City Research Online so that its users may access the research outputs of City University London's staff. Copyright © and Moral Rights for this paper are retained by the individual author(s) and/ or other copyright holders. All material in City Research Online is checked for eligibility for copyright before being made available in the live archive. URLs from City Research Online may be freely distributed and linked to from other web pages.

Versions of research

The version in City Research Online may differ from the final published version. Users are advised to check the Permanent City Research Online URL above for the status of the paper.

Enquiries

If you have any enquiries about any aspect of City Research Online, or if you wish to make contact with the author(s) of this paper, please email the team at publications@city.ac.uk.

1
2
3
4
5
6
7
8
9
10
11
12
13
14
15
16
17
18
19
20
21
22
23
24
25
26
27
28
29
30
31
32
33
34
35
36
37
38
39
40
41
42
43
44
45
46
47
48
49
50
51
52
53
54
55
56
57
58
59
60
61
62
63
64
65

Stimulation and measurement patterns versus prior information for fast 3D EIT: A breast screening case study

Panagiotis Kantartzis^{a,*}, Montaserbellah Abdi^a, Panos Liatsis^a

^a*Information Engineering and Medical Imaging Group, EEIE, SEMS, City University London, Northampton Square, EC1V 0HB, London, UK*

Abstract

Imposing prior information is a typical strategy in inverse problems in return for a stable numerical algorithm. For a given imaging system configuration, the Picard stability condition could then be deployed as a practical measure of the performance of the system against noise contaminated data. Herein, we make extensive use of the above measure to quantify the performance of impedance imaging systems for various stimulation protocols. We numerically demonstrate that a large number of electrodes, as required for breast imaging, adds little value, if any, to the performance of the impedance imaging system. On the other hand, by engaging more electrodes to the 3D firing process, a step increase in performance is recorded. Numerical results on a female breast phantom reveal that for a conventional combination of stimulation and prior information, the potential of the imaging system is approximately 15%. In contrast, for the proposed stimulation and a better prior,

*Corresponding author at: Information Engineering and Medical Imaging Group, EEIE, SEMS, City University London, Northampton Square, EC1V 0HB, London, UK, Tel: +44 (0) 207040 3886, FAX: +44 (0) 207040 8568

Email address: p.kantartzis@city.ac.uk (Panagiotis Kantartzis)

1
2
3
4
5
6
7
8
9 recorded performance is 61% and 97%, respectively. Finally, since a smaller
10 number of electrodes participate in the measurement process, a significantly
11 reduced number of observable data is acquired. It is worth underlining, that
12 despite the reduction in measurements no compromise in the quality of the
13 reconstructed image is reported.

14
15
16
17
18 *Keywords:* Electrical Impedance Tomography, stimulation protocol,
19 measurement protocol, SVD, Picard's criterion, breast screening
20
21
22

23 24 **1. Introduction**

25
26
27
28
29
30
31
32
33
34
35
36
37
38
39
40
41
42
43
44
45
46
47
48
49
50
51
52
53
54
55
56
57
58
59
60
61
62
63
64
65

2 Despite the advances in medicine and diagnostic technology, cancer is
3 still one of the top causes of death, if not the leading one on the global
4 scale. WHO, the World Health Organisation, on its February 2012 fact
5 sheet, reports that '*deaths from cancer worldwide are projected to continue*
6 *to rise to over 13.1 million in 2030*' [1]. In particular, lung, stomach, liver,
7 colon and breast cancer cause the most cancer deaths each year.

8 In the UK alone, '*breast cancer is the second biggest cause of death from*
9 *cancer for women, after lung cancer. On average, nearly 50,000 people are*
10 *diagnosed with breast cancer each year. That is one person every 10 min-*
11 *utes*' [2]. As breast cancer is one of the most common cancer types and has
12 higher cure rates if detected early [1], there is an all-time-high interest in the
13 development of fast & robust screening modalities for breast cancer.

14 The gold standard for breast screening is essentially Mammography, often
15 coupled with Magnetic Resonance Imaging (MRI). However, both Mammog-
16 raphy and MRI suffer from low specificity rates [3, 4]. In fact, a relatively high
17 rate of raising false positive screenings is frequently encountered, entailing

1
2
3
4
5
6
7
8
9
10
11
12
13
14
15
16
17
18 additional costs for the healthcare system but, more importantly, additional
19 distress for the patient. One should also factor in that patients subject to
20 Mammography screening are exposed to ionizing radiation.

21 On the other hand, in breast MRI, a contrast agent need to be used [5],
22 also known to produce toxic side effects for the patients. In addition, in
23 younger ages where the breast tissue is denser, Mammography fails to pick
24 abnormalities so Ultrasound appears to be more appropriate [6]. Therefore,
25 as specificity of current imaging modalities is not adequate, further develop-
26 ment of alternative techniques is highly desirable. Herein, we omit to discuss
27 methods not fully-approved by the US Food and Drug Administration as
28 screening tools for breast cancer, e.g., Thermography, CT Laser Mammog-
29 raphy.

30 Electrical Impedance Tomography (EIT) is also being investigated in the
31 field of breast imaging as a complementary technique to Mammography for
32 breast cancer detection. Unlike MRI, EIT is portable, inexpensive and in
33 a similar spirit to Ultrasound it does not use ionizing radiation. It is also
34 worth underlining that EIT is already successful in providing valuable in-
35 sight in both industrial and medical applications [7]. Moreover, commercial
36 versions of EIT systems are now available in routine clinical use [8]. As the
37 electrical properties of normal and malignant breast tissue differ [9], an early
38 commercial development for breast screening, T-scan, has been developed
39 [10]. T-scan has received approval by the US Food and Drug Administration
40 to be used as a diagnostic aid to Mammography as it has been demonstrated
41 to improve sensitivity and specificity. Hence, there is an all-time-high interest
42 in further pursuing research to establish whether EIT could further improve

1
2
3
4
5
6
7
8
9
10 43 reported specificity rates, if not survive as a stand alone screening modality
11 44 in this field.

12
13 45 In principle, EIT is simple and easy to operate and requires no expe-
14 46 rienced clinicians to perform a scan. In a typical experiment, currents are
15 47 applied through electrodes attached to the periphery of a body and voltage
16 48 measurements are collected from some other surface electrodes. The observed
17 49 data vector, i.e., voltage measurements, is then fed to a computer to estimate
18 50 the interior material (tissue) distribution [11–15].

19
20
21
22
23
24 51 Not many will argue that most of the numerical effort is typically allo-
25 52 cated to the image reconstruction aspects of the EIT problem. Unlike stan-
26 53 dard imaging methods, as for instance xray-CT, in EIT one could model,
27 54 study and demonstrate how a ‘local’ perturbation affects not only nearby
28 55 measurements but, crucially, all measurements [11]. Despite the fact that
29 56 captured measures are sensitive to local perturbations, little is reported on
30 57 how to optimise driving patterns that produce more valuable measurements
31 58 and thus reconstructions. Recall that measurements is the only observable
32 59 data vector.

33
34
35
36
37
38
39
40
41 60 It is worth mentioning the reports [16, 17], where the authors derived pat-
42 61 terns that maximise the distinguishability between two corresponding mate-
43 62 rials or simply the anticipated reconstruction contrast. Briefly, the idea is to
44 63 maximise the difference between the two Neuman-to-Dirichlet (NtD) maps.
45 64 In a circular domain, the optimal stimulation pattern accounts for the eigen-
46 65 values of the corresponding NtD functional, i.e., firing on electrodes with
47 66 Fourier bases. Although this provides an excellent solution from a mathe-
48 67 matical point of view, there are some practical limitations of the suggested

1
2
3
4
5
6
7
8
9
10
11
12
13
14
15
16
17
18
19
20
21
22
23
24
25
26
27
28
29
30
31
32
33
34
35
36
37
38
39
40
41
42
43
44
45
46
47
48
49
50
51
52
53
54
55
56
57
58
59
60
61
62
63
64
65

68 method. For instance, one needs to drive a pattern on all electrodes and then
69 measure the resulting voltages on same (current carrying) electrodes. Hence,
70 more practical patterns are sought.

71 In a 3D setting, there is a greater flexibility in stimulating the object.
72 The authors in [18], suggested some measures to assess available stimulation
73 protocols. Amongst many, their findings encouraged non-adjacent electrode
74 patterns. Further, since for a given set of driving patterns, measurements are
75 subject to a reconstruction (and thus regularisation) algorithm, results could
76 be significantly enhanced or deteriorated. It is not clear therefore, how to
77 best stimulate an object in order to get the most out of a measurement data
78 set. This simply means, that the way that the object is stimulated could
79 either enhance or obscure information content. See [19] for a discussion on
80 information content for EIT.

81 In the context of breast imaging, the reconstruction situation could be
82 much less trivial mainly due to practical limitations. For instance, a large
83 array of electrodes needs to be attached to the easily deformable female
84 breast. Since both the number of electrodes and hence measurements as
85 well as model misfits of the actual boundary surface are said to affect the
86 quality of the reconstructed image [20], one encounters a potential bottleneck
87 on how to proceed. The latter can be addressed by optical measurements
88 that could result in accurate representations of the female breast surface [21].
89 However, there is no straightforward way as to which stimulation pattern
90 would provide best results for the breast domain at hand and, of course,
91 under what constraints.

92 To alleviate this, the authors in [22] proposed plane-wise sinusoidal volt-

1
2
3
4
5
6
7
8
9
10 93 age patterns with different phases per plane, that provide improved images.
11 94 Assuming that a phase difference is the way forward for breast EIT screening,
12
13 95 the question on whether one takes the most out of the available EIT system,
14
15 96 as some of the measurements are (numerically) linearly dependent, is still
16
17 97 open. In sort, this implies that one would eventually need to compensate
18
19 98 for this loss by means of penalising higher frequency solutions, i.e., regular-
20
21 99 isation, to avoid numerical instability. Needless to say that determining the
22
23 100 optimal number of electrodes is also an additional open issue.

24
25 101 In the same spirit, the authors in [23] identified the stimulation short-
26
27 102 comings and proposed a much promising strategy which was numerically
28
29 103 demonstrated in a 2D setting with 32 electrodes. Unlike most conventional
30
31 104 methods reported in literature, the novelty lies in engaging 4 electrodes to
32
33 105 act as group and then use 2 such groups of 4 electrodes to drive a current pat-
34
35 106 tern. The authors, by means of Generalised Singular Value Decomposition
36
37 107 (GSVD), derived a measure to quantify collected measurements against prior
38
39 108 information as well as measurement noise, in order to filter out problematic
40
41 109 singular values.

42
43 110 In this paper, we follow the guidelines of [23], as, in our view, this ap-
44
45 111 pears to be the only practical measure that factors in prior information when
46
47 112 devising a stimulation strategy. Further, we extend the stimulation protocol
48
49 113 to 3D, where a greater number of electrodes and patterns is often available.
50
51 114 To the best of our knowledge, this methodology has never been tested to a
52
53 115 3D domain before. On the other hand, our contribution differs from the one
54
55 116 in [23] as we account for groups of variable electrode numbers to apply the
56
57 117 desired stimulation protocol. This implies a variable reduction in the num-

1
2
3
4
5
6
7
8
9
10
11
12
13
14
15
16
17
18
19
20
21
22
23
24
25
26
27
28
29
30
31
32
33
34
35
36
37
38
39
40
41
42
43
44
45
46
47
48
49
50
51
52
53
54
55
56
57
58
59
60
61
62
63
64
65

118 ber of collected measurements (and thus data acquisition timings) without
119 compromising on the quality of the reconstructed images. Finally, there is
120 no need to measure on current carrying electrodes, e.g., [16, 22].

121 In the next section, a brief introduction to the theoretical framework
122 of EIT is given. The Singular Value Decomposition (SVD) along with the
123 GSVD are also provided as a means of studying a reconstruction stability
124 criterion (Picard’s criterion) in Section 3. Next, the suggested 3D stimulation
125 scheme is demonstrated in Section 4 on a simple cylindrical tank and perfor-
126 mance is reported against conventional stimulation patterns. The method-
127 ology is then carried over to Section 5 which is concerned with a female
128 breast phantom, where further numerical results are presented. Discussion
129 and conclusions finalise this article.

130 **2. Theory: EIT problem**

131 The goal in EIT is to successfully derive a stable numerical map between
132 observable voltages and unobservable interior admittivity distribution(s) in
133 order to infer desirable material/tissue information.

134 There are two computational models in literature for the EIT; a higher
135 frequency one [24] and a lower frequency one [25]. The latter is freely avail-
136 able from the EIDORS repository [26] whilst, nowadays, represent a widely
137 accepted and used testbench. Therefore, without loss of generality, we omit
138 the high-frequency model and we focus on the low-frequency one.

139 *2.1. The forward problem*

140 According to the EIT-adapted adjoint fields method [27], the process of
141 simulating the boundary surface electrode voltages (i.e., assembling the so

1
2
3
4
5
6
7
8
9
10
11
12
13
14
15
16
17
18
19
20
21
22
23
24
25
26
27
28
29
30
31
32
33
34
35
36
37
38
39
40
41
42
43
44
45
46
47
48
49
50
51
52
53
54
55
56
57
58
59
60
61
62
63
64
65

142 called forward operator in EIT) requires repeated solutions of a generalised
143 Laplacian PDE of non-constant coefficient, subject to appropriate boundary
144 conditions [28] of the form

$$\begin{aligned} \nabla \cdot (\sigma \nabla u) &= 0 && \text{in } \Omega \\ \sigma \nabla u \cdot \nu &= \iota && \text{on } \Gamma \\ u + z_\ell \sigma \nabla u \cdot \nu - U_\ell &= 0 && \text{on } \Gamma_\ell \end{aligned} \quad (1)$$

145 where $\sigma, u, U_\ell, \nu, \iota, z_\ell$ are the admittivity, the interior potential distribution,
146 the surface potential on the ℓ -th electrode, the outward unit normal vec-
147 tor, the current density and the surface impedance, respectively. Additional
148 boundary conditions on the interelectrode gaps Υ require that

$$\sigma \nabla u \cdot \nu = 0 \quad \text{on } \Upsilon. \quad (2)$$

149 $\Omega \subset \mathbb{R}^3$ is a bounded domain equipped with L electrodes attached on its
150 Lipschitz boundary surface $\partial\Omega$. $\Gamma \subset \partial\Omega$ is the union of areas under each
151 electrode, assumed to be open connected subsets $\bigcup_{\ell=1}^L \Gamma_\ell = \Gamma$, whose closures
152 are disjoint, $\bigcap_{\ell=1}^L \bar{\Gamma}_\ell = \emptyset$. $\Upsilon := \partial\Omega \setminus \Gamma$ is the union of the remaining areas.
153 Defining the sesquilinear form as [28]

$$a_\Omega((v, V), (w, W)) := \int_\Omega \sigma \nabla v \cdot \nabla \bar{w} \, d\Omega + \sum_{\ell=1}^L \int_{\Gamma_\ell} \frac{1}{z_\ell} (v - V_\ell) (\bar{w} - \bar{W}_\ell) \, ds_{\Gamma_\ell}, \quad (3)$$

154 the weak formulation of the EIT problem on the original domain Ω can be
155 stated as the following direct Boundary Value Problem (BVP): Given a (c -
156 th) driving pattern (currents) $I^{(c)} := (I_1, \dots, I_L)^T \in \mathbb{R}^L$ find $(u, U) \in \mathcal{H}_\Omega^1$
157 such that

$$a((u, U), (v, V)) = \sum_{\ell=1}^L I_\ell \bar{V}_\ell \quad \text{for all } (v, V) \in \mathcal{H}_\Omega^1 \quad (4)$$

1
 2
 3
 4
 5
 6
 7
 8
 9
 10 where I_ℓ denotes the current applied to the ℓ -th electrode and $\mathcal{H}_\Omega^1 := \{\mathcal{H}^1(\Omega) \oplus$
 11 $\mathfrak{S}^L\}/\mathfrak{S}$ is the (quotient) solution space. Equation (4) requires repeated so-
 12 lutions for the various driving patterns $I^{[d]} := (I^{(1)}, I^{(2)}, \dots, I^{(d)}) \in \mathbb{R}^{L \times d}$
 13 that form the stimulation pattern $I^{[d]}$. In addition, solutions of m -adjoint
 14 stimulation patterns $I^{[m]} \in \mathbb{R}^{L \times m}$ are also required [27]. Intuitively, varying
 15 the number of stimulation patterns directly affects the number of required
 16 solutions for the PDE, Equation (4). Given that EIT is typically concerned
 17 with large-scale Finite Element systems, ‘short’ patterns ($d \ll$) are favoured
 18 as they offer significant computational savings. Hence, it is not hard to infer
 19 that the role of the stimulation pattern $I^{[d]}$ (and eventually $I^{[m]}$) is of great
 20 computational significance.
 21
 22
 23
 24
 25
 26
 27
 28
 29

30 Using conventional EIT modelling methods, measured data y is essentially
 31 the result of the application of a measurement operator M (Green’s operator)
 32 to electrode potentials U from Equation (4) as
 33
 34
 35
 36
 37
 38

$$y = MU \tag{5}$$

39
 40
 41 The steps above essentially reflect the so-called forward EIT problem and
 42 are summarised by the non-linear operator $\Lambda : L_2(\Omega) \rightarrow \mathfrak{S}^m$,
 43
 44
 45
 46
 47
 48

$$\Lambda(\sigma) = y \tag{6}$$

49
 50
 51 which links the interior material distribution $\sigma := \sigma(\mathbf{x}) \in L_2(\Omega)$, $\mathbf{x} \in \Omega$ with
 52 the observed data $y \in \mathfrak{S}^m$, where m is the number of measurements. Of
 53 interest for EIT imaging is the inverse problem, set out in the next section.
 54
 55
 56
 57
 58
 59
 60
 61
 62
 63
 64
 65

1
2
3
4
5
6
7
8
9
10 177 *2.2. The inverse problem*

11 The inverse EIT problem is formed as the problem of estimating the
12 unobserved distribution σ from an observable one y . From an optimisation
13 point of view, this can be formed as a quadratic minimisation functional of
14 the form
15
16
17
18
19
20
21

$$22 \min_{\sigma} \frac{1}{2} \|\Lambda(\sigma) - y\|_2^2 \quad (7)$$

23
24
25 182 *2.3. The linearised EIT problem*

26 Given a neighbourhood σ_0 , the forward operator is said to be Fréchet
27 differentiable, hence application of Taylor's expansion yields the linearised
28 version of the EIT functional as
29
30
31
32
33

$$34 \underbrace{\Lambda^{(1)}(\sigma_0)}_J \underbrace{(\sigma - \sigma_0)}_{\delta\sigma} = \underbrace{(\Lambda(\sigma) - \Lambda(\sigma_0))}_{\delta y} + \underbrace{O(\sigma^2)}_{\approx 0} \quad (8)$$

35
36
37
38
39 186 or approximately as

$$40
41
42
43
44 J\delta\sigma = \delta y \quad (9)$$

45
46
47 187 where $\Lambda^{(1)}(\sigma_0)$ is essentially the first order Fréchet differentiation of the non-
48 linear operator Λ at σ_0 . Clearly, the dimensionality of J is determined by
49 the dimensionality of the unobservable distribution σ and the measured data
50
51
52
53 190 y .

1
2
3
4
5
6
7
8
9
10 191 *2.4. Measured data*

11 In a typical EIT fashion, the measured data vector is contaminated with
12 some noise originating from various physiological, modelling and discretisa-
13 tion errors. Without loss of generality, herein, noise ϵ is assumed as additive.
14
15
16
17 As such,
18

$$J\delta\sigma = \delta y + \epsilon \quad (10)$$

19 In a discrete setting, where only a finite set of measurements (y) could be
20 collected, the number of the corresponding discretised equations of Equation
21 (10) is finite. On the other hand, since the number of discretisation variables
22 for σ typically outnumber the dimensionality of the measurements, one en-
23 counters a heavily underdetermined problem. From a least squares point of
24 view, the (maximum likelihood) analytical solution of the above system results
25 in the solution of the normal set of equations as
26
27
28
29
30
31
32
33
34
35
36
37
38
39

$$\delta\sigma = (J^T J)^{-1} J^T (\delta y + \epsilon) \quad (11)$$

40
41
42
43 Unfortunately, the above solution is of little practical numerical use as
44 the discrete equivalent of J , i.e., \mathbf{J} , is a dense, rectangular and ill-conditioned
45 matrix, hence sensitive to numerical errors. Using simple algebra, it is not
46 hard to demonstrate that since \mathbf{J} is anticipated to be ill-conditioned, $(\mathbf{J}^T \mathbf{J})$
47 is severely ill-conditioned. Hence, one would eventually need to account for
48 this numerical deficiency by means of a regularisation functional R in order
49 to compute a physically meaningful solution. The minimisation functional is
50 now casted as
51
52
53
54
55
56
57
58
59
60
61
62
63
64
65

$$\min_{\sigma} \frac{1}{2} \|J\delta\sigma - \delta y\|_2^2 + R(\sigma) \quad (12)$$

211 In the Tikhonov regime, typical regularisation candidates are constraints
 212 for a bounded solution $R(\sigma) := \frac{1}{2}\lambda\|\sigma\|_2^2$ or, more precisely, for a bespoke
 213 penalisation of non-smooth solutions as $R(\sigma) := \frac{1}{2}\lambda\|D\sigma\|_2^2$, where λ is a
 214 regularisation parameter, D is a differential operator. The selection of the
 215 optimal regularisation parameter and matrix is beyond the scope of this arti-
 216 cle and is omitted. The reader is kindly referred to [29] for the determination
 217 of the λ using, e.g., the L-curve method.

218 Assuming a Tikhonov based regularisation functional, one now arrives at
 219 the (maximum a posteriori) analytical solution

$$\delta\sigma = (J^T J + \lambda D^T D)^{-1} J^T (\delta y + \epsilon) \quad (13)$$

220 A discussion on non-linear reconstruction methods is omitted. Rather,
 221 we refer to [30] and references therein for extensive reviews and discussions.

222 2.5. SVD & GSVD

223 In the sequel, the δ -term in the discrete equivalents of $\delta\sigma$, δy , is dropped
 224 for notational convenience. Also, real admittivities are now assumed, i.e.,
 225 conductivities.

226 The SVD is now employed to facilitate discussion on the interaction be-
 227 tween original information contents encapsulated in \mathbf{J} and the artificially
 228 imposed prior information matrix \mathbf{R} . SVD analysis involves expansion of the
 229 linearised system to an orthogonal basis as in the standard Fourier analysis.

1
2
3
4
5
6
7
8
9
10 230 The SVD of the (linearised) discrete forward operator $\mathbf{J} \in \mathfrak{R}^{m \times N}$, $m \geq N$, is
11 231 effectively a decomposition of the form [31]

$$\mathbf{J} = \mathbf{P}\mathbf{\Xi}\mathbf{Q}^T = \sum_{i=1}^N \mathbf{p}_i \xi_i \mathbf{q}_i^T \quad (14)$$

12
13
14
15
16
17 232 where $\mathbf{P} = (\mathbf{p}_1, \mathbf{p}_2, \dots, \mathbf{p}_m)$ and $\mathbf{Q} = (\mathbf{q}_1, \mathbf{q}_2, \dots, \mathbf{q}_N)$ are matrices with or-
18 233 thonormal columns, i.e., $\mathbf{P}^T \mathbf{P} = \mathbf{Q}^T \mathbf{Q} = \mathbf{I}$, called the left and right singular
19
20
21 234 vectors, respectively. The non-negative entries of the diagonal matrix $\mathbf{\Xi}$ are
22
23 235 typically sorted in non-increasing order as

$$\xi_1 \geq \xi_2 \geq \dots \xi_N \geq 0 \quad (15)$$

24
25
26
27
28
29 236 and are identified as the ‘singular’ values.

30
31
32 237 In broad terms, the sequential order of the singular values is inversely
33
34 238 proportional to information fidelity. Coarse information, associated with low
35
36 239 frequencies, is anticipated towards the first singular values, whilst fine detail,
37
38 240 encapsulated in high frequencies, is usually concentrated towards the last
39
40 241 singular values, i.e., as $i \rightarrow N$.

41
42 242 Using SVD, one may determine a generalised inverse \mathbf{J}^\dagger for \mathbf{J} , correspond-
43
44 243 ing to the different properties that \mathbf{J} may satisfy. In effect, one may obtain
45
46 244 \mathbf{J}^\dagger as

$$\mathbf{J}^\dagger = \sum_{i=1}^{n_\dagger} \mathbf{q}_i \xi_i^{-1} \mathbf{p}_i^T \quad (16)$$

47
48
49
50
51 245 where

$$n_\dagger := \begin{cases} N, & \text{if } \mathbf{J} \text{ is invertible;} \\ n_r = \text{rank}(\mathbf{J}), & \text{if } \mathbf{J} \text{ is } r\text{-rank-deficient.} \end{cases} \quad (17)$$

1
2
3
4
5
6
7
8
9
246 The first case assumes that \mathbf{J} is of full rank and effectively corresponds to
10
247 the so called generalised Moore-Penrose ‘pseudo inverse’ [31]. The second
11
12
248 case, which reflects the EIT problem, \mathbf{J} is assumed to be r -rank deficient
13
14
249 which implies that some of the smallest singular values are practically zero,
15
16
250 i.e.,

$$\xi_1 \geq \dots \xi_{n_r} \geq \xi_{n_r+1} \approx \dots \approx \xi_N \approx 0 \quad (18)$$

251 Based on SVD, the Moore-Penrose inverse \mathbf{J}^\dagger can be written in the fol-
22
23
24
252 lowing form [29]

$$\boldsymbol{\sigma}_\dagger = \mathbf{J}^\dagger \mathbf{y} = \sum_{i=1}^{n_\dagger} \frac{\mathbf{p}_i^T \mathbf{y}}{\xi_i} \mathbf{q}_i \quad (19)$$

253 From the above equation, one may study the contribution of the singular
31
32
33 values ξ_i and the solution $\boldsymbol{\sigma}_\dagger$ and in fact, understand why SVD provides
34
254 an insight into the ill-posedness. Generally speaking, should one attempt to
35
255 invert small singular values $\xi_i \approx 0$, the solution $\boldsymbol{\sigma}_\dagger$ would attract considerably
36
256 high values, effectively obscuring the desired solution. In this respect, even a
37
257 small perturbation in \mathbf{y} can cause a dramatically high perturbation in $\boldsymbol{\sigma}_\dagger$ as
38
258 the tiny values of ξ_i would eventually prevail, rendering the obtained solution
39
40
259 meaningless.
41
42
43
44
260

261 An indication of the severity of ill-conditioning is given by the ratio of
45
46
47 the largest to the smallest singular value $\kappa_{\mathbf{J}} = \xi_1/\xi_N$ which is also identified
48
262 as the condition number. The larger the condition number of \mathbf{J} , the more
49
50
263 severe the ill-posedness of the problem and the more the ill-conditioning it is.
51
52
264 The concept of GSVD is now considered, where the main difference between
53
54
265 GSVD and SVD is that, rather, a matrix pair is now analysed. In this light,
55
56
266

1
2
3
4
5
6
7
8
9
267 GSVD provides valuable insight of a matrix coupling. For our needs, the
10
268 coupling of \mathbf{R} , i.e., the selected regularisation matrix, and \mathbf{J} is assumed. In
11
12
13 269 the GSVD setting, the decomposition takes place in a slightly different form
14
15 270 for the individual matrices as

$$\mathbf{J} = \mathbf{P}\mathbf{\Xi}\mathbf{X}^{-1}, \quad \mathbf{R} = \mathbf{Q}\mathbf{M}\mathbf{X}^{-1} \quad (20)$$

21
22 where matrix \mathbf{X} is non-singular and \mathbf{P} , \mathbf{Q} are orthonormal and different
23
24 272 from their SVD counterparts. This notational abuse is solely for convenience
25
26 273 purposes. In a similar fashion to SVD, matrices $\mathbf{\Xi}$ and \mathbf{M} are diagonal with
27
28 274 normalised entries $\xi_i, \mu_i, i = 1, \dots, p, \xi_i^2 + \mu_i^2 = 1$ and for historical reasons
29
30 275 arranged in non-decreasing and non-increasing order $0 \leq \xi_i \leq 1, 1 \leq \mu_i \leq 0$,
31
32 276 respectively. The generalised singular values are then

$$\gamma_i = \frac{\xi_i}{\mu_i} \quad (21)$$

33
34
35 277 In a similar fashion to SVD, one could study the generalised singular
36
37
38 278 values to assess ill-conditioning, however, by taking into account prior infor-
39
40 279 mation.

280 3. Picard's stability condition

41
42
43
44
45 281 In [29], the author popularised Picard's criterion as an invaluable insight
46
47 282 into the stability of the regularisation problem. In effect, in Picard's crite-
48
49 283 rion the stability of the regularised problem is oriented around the (decay of)
50
51 284 Fourier coefficients $|\mathbf{p}_i^T \mathbf{y}|$, or more realistically $|\mathbf{p}_i^T (\mathbf{y} + \boldsymbol{\epsilon})|$ [29]. These coef-
52
53 285 ficients are frequently encountered in the literature as Picard's coefficients.
54
55 286 Herein, we adopt this term.
56
57
58
59
60
61
62
63
64
65

1
2
3
4
5
6
7
8
9
10 287 As thoroughly discussed in [29], the key feature exploited in this section is
11 288 that our measurements are contaminated with noise. It turns out that such
12
13 289 errors typically tend to have components along all the left singular vectors
14
15 290 \mathbf{p}_i . Hence, Picard's coefficients $|\mathbf{p}_i^T(\mathbf{y} + \boldsymbol{\epsilon})|$ of observed data, typically level
16
17 291 off around the noise measurement levels. Therefore, in order to maintain
18
19 292 stability, one requires that Picard's coefficients decay to zero faster than the
20
21 293 generalised singular values γ_i .

22
23 294 This is a great computational quality 'measure', that couples observed
24
25 295 data with a priory information (incorporated in the regularisation matrix),
26
27 296 without requiring to execute the reconstruction algorithm, e.g., Equation
28
29 297 (13). In this regard, it is an *a priory criterion* to comment on the quality, if
30
31 298 not effectiveness, of the proposed EIT configuration. Nevertheless, Picard's
32
33 299 criterion is a computationally intense, especially for large scale systems as it
34
35 300 involves GSVD. On the positive side, one would only need to run this test
36
37 301 once and in advance of the reconstruction algorithms, in order to test the
38
39 302 suitability of the chosen regularisation matrix for the problem at hand.

40
41 303 In the next section, we scrutinise stimulation patterns under Picard's
42
43 304 stability criterion.

305 4. Putting everything together: Stimulation, measurements & nu- 306 merical stability

307
308 In order to provide a fair comparison between conventional and proposed
309
310 stimulation, we kick off our numerical simulation with a simple study: We
311
312 consider a cylindrical tank of uniform background distribution and a spher-
313
314 ical perturbation $(x_1 + .2)^2 + (x_2 + .3)^2 + (x_3 + .4)^2 - .1^2 < 0$ of $\delta\sigma = 10\%$

1
 2
 3
 4
 5
 6
 7
 8
 9 of the background value. One could consider adjacent simulations, however
 10 according to [18] little information is acquired with adjacent stimulation pat-
 11 terns so we focus on a standard opposite 2-electrode pair stimulation pattern.
 12
 13 For clarity, we opt for a linearised problem, the solution of which is given by
 14 Equation (13). Unless otherwise specified, the identity matrix is employed as
 15 the regularisation prior, $\mathbf{R}^T \mathbf{R} = \mathbf{I}$. At this stage, the selection of the regu-
 16 larisation matrix is of secondary importance when compared to the selection
 17 stimulation pattern. Next, we vary the number of electrode ring number as
 18 well as the number of electrodes per ring. In all simulation results, 25dB
 19 Gaussian noise ϵ is added to the simulated measurements.
 20
 21
 22
 23
 24
 25
 26
 27
 28

321 4.1. Simple cylindrical phantom, 2-electrode pair

322 When $L := 6$ electrodes are available and current is applied to a 2-
 323 electrode pair of opposite electrodes, i.e., $I_1 = [1, 0, 0, -1, 0, 0]^T$, one could
 324 collect measurements between electrodes $\{2, 3\}$ and $\{5, 6\}$, i.e., $(L - 4)$ mea-
 325 surements for this particular current pattern. By shifting the current pat-
 326 tern by one electrode, one arrives at $I_2 = [0, 1, 0, 0, -1, 0]^T$. Repeating for
 327 L -electrodes, eventually, one could potentially collect $m := (L - 4)L = 12$
 328 measurements, half of which are linearly dependent. Thus, one practically
 329 collects a total of $m := L(L - 4)/2 = 6$ measurements for \mathbf{y} .

330 Assuming a piecewise constant (per element) approximation in (3), (4),
 331 for the real admittivity distribution,

$$\sigma \approx \sum_i^N \sigma_i \chi_{i=1} \tag{22}$$

332 where χ_i is the characteristic function and N is the number of elements, the
 333 size of the typically underdetermined version of the Jacobian is $\mathbf{J} \in \mathfrak{R}^{m \times N}$,

1
2
3
4
5
6
7
8
9
10 334 where practically $m \ll N$. The sensible step therefore is to establish means
11 335 of increasing the number of measurements m until, ideally, $m \approx N$. This,
12
13 336 in turn, entails a significant increase in the number of measurements and,
14
15 337 eventually, electrodes L .

16
17 338 Aside from impractical, an increased number of measurements m will con-
18
19 339 tribute towards unrealistically high computational overheads both for the as-
20
21 340 sembly and inversion of the dense matrix \mathbf{J} (not to mention ill-conditioning).
22
23 341 Therefore, should a classical 2-pair stimulation and measurement strategy
24
25 342 be deployed, a practical upper bound in terms of available computational
26
27 343 resources is encountered.

28
29 344 On the other hand, taking into account that we are dealing with an
30
31 345 inverse problem, it is essential for stability to only utilise a subset of the
32
33 346 available singular values spectrum, as suggested by the singular value analysis
34
35 347 of Section 2.5. Moreover, in order to factor in the role of the regularisation
36
37 348 matrix \mathbf{R} as well as the presence of the noise in the measurements, the GSVD
38
39 349 analysis, in particular, is recalled.

40
41 350 In Figure 1a), a plot of Picard's coefficients along with the generalised
42
43 351 singular values γ_i is illustrated for 3 rings of electrodes. Recalling Picard's
44
45 352 criterion of Section 3, one requires a faster decay of Picard's coefficients
46
47 353 $|\mathbf{p}_i^T(y + \epsilon)|$ than the decay of the generalised singular values γ_i . In [23], the
48
49 354 ratio of the generalised singular values that meet Picard's criterion over the
50
51 355 total number of available generalised singular values is termed as *gain* of the
52
53 356 selected stimulation pattern. Clearly, as it can be depicted from Figure 1a),
54
55 357 the majority of singular values is below Picard's threshold. This becomes
56
57 358 profound as the number of electrodes increases in the same Figure for the

1
2
3
4
5
6
7
8
9
10 359 cases of b) 24, c) 36 and d) 48 electrodes, where notably only a few singular
11 360 values γ_i survive filtration. The actual gain recorded for each case, when 3
12 ring of electrodes are considered, is tabulated in Table 1 and termed as **Gain**
13 361 **1**. In the same Table, the ratio of the number of electrodes over the number
14
15 362 **1**. In the same Table, the ratio of the number of electrodes over the number
16
17 363 of measurements is also tabulated to demonstrate how impropotional the
18
19 364 increase of electrodes is with respect to measurements could be.

20
21 365 In order to further demonstrate that, practically, the quality of gathered
22
23 366 measurements is no better when additional electrode rings are added, we
24
25 367 repeat the previous experiment. In the new configuration, the number of
26
27 368 electrodes remains fixed for each case as before, however, an additional ring
28
29 369 of electrodes is allowed. As such, a different electrode distribution is enabled
30
31 370 as illustrated in Figure 2. The corresponding gains for the 4-ring systems are
32
33 371 now tabulated in Table 2 and termed as **Gain 2**. By coupling Figure 2 and
34
35 372 Table 2, it is evident that, assuming fixed number of electrodes for each case,
36
37 373 essentially the additional ring allowance, offers very little improvements, if
38
39 374 any at all.

40 375 Taking into account that the meshing algorithm [32], produces slightly
41
42 376 more mesh elements to accommodate the need for the additional ring, gains
43
44 377 obtained from **Gain 2** are slightly worse than the ones obtained in **Gain 1**
45
46 378 or, in broad terms, in the same range as in **Gain 1**. It is not hard to obtain
47
48 379 from Tables 1 & 2 that the additional ring of electrodes results in the same
49
50 380 number of measurements and does not yield an overall system improvement
51
52 381 in the sense discussed herein.

53 382 In fact, one should focus on the fact that, for the given opposite 2-
54
55 383 electrode pair stimulation pattern, as the total number of electrodes increases,
56
57
58
59
60
61
62
63
64
65

1
2
3
4
5
6
7
8
9
10 384 both **Gain 1** & **Gain 2** plummet, as more regularisation would indeed be
11 385 required for stability. In this regard, less singular values would escape fil-
12 386 tration. This should be approached as a numerical acknowledgement of the
13 387 fact that increasing the number of electrodes does not (necessarily) increase
14 388 the potential information content. Note that this acknowledgement triggers
15 389 again the earlier question on whether we take the most out of an EIT system,
16 390 which essentially paves the way for non-conventional stimulation/collection
17 391 protocols.

18 392 *4.2. Simple cylindrical phantom - multiple electrode pair*

19 393 Rather than engaging two electrodes to stimulate currents, we employ
20 394 a multiple-electrode stimulation pair. That is, opposite *groups of electrodes*
21 395 are now considered. In order to briefly report on the rationale behind this
22 396 step, assume that $L = 12$ electrodes are available at our disposal and that
23 397 the number of desired stimulation patterns is $d = 6$. We now suitably group
24 398 some of the available electrodes, say 1 group of 2 electrodes, where current
25 399 is injected, and 1 group of 2 electrodes where current exits the medium. In
26 400 this way, we are left with $L - 2 \cdot 2 - 2 = 6$ non-current carrying electrodes to
27 401 gather measurement data. For 6 desired patterns this accounts for $6 \cdot 6 = 36$
28 402 measurements. This figure is significantly less than the 96 measurements
29 403 that would have otherwise needed. The advantage of this stimulation pat-
30 404 tern is that although $L = 12$ electrodes were originally considered, the EIT
31 405 system is essentially clocked with just 36 measurements. In other words, 36
32 406 measurements translate to just 37.5% of the overall time required to collect
33 407 data with the conventional 2-pair opposite protocol.

34 408 Given the GSVD discussion of the previous sections, it remains to demon-

1
2
3
4
5
6
7
8
9
10 409 strate that the resulting gain for the multiple-electrode pair is better than
11 410 the conventional one. Intuitively, since more electrodes are involved in the
12
13 411 firing process whilst occupying a greater boundary surface, it is sensible to
14
15 412 anticipate some gain improvements over the conventional 2-electrode pair
16
17 413 stimulation scheme. In other words, one would expect to observe a faster de-
18
19 414 cay in Picard's coefficients than the generalised singular values of the matrix
20
21 415 pair (\mathbf{J}, \mathbf{I}) for this particular case.

22
23 416 Figure 3 reveals the generalised singular spectrum against Picard's coeffi-
24
25 417 cients. The superiority of the proposed scheme materialises from the readings
26
27 418 of Table 3, in particular when a large number of electrodes L is considered
28
29 419 (**Gain 3**). The naive interpretation of Table 3 is that for the same domain,
30
31 420 with the same forward problem parameters and the same regularisation ma-
32
33 421 trix, one could essentially derive an improved system. As in the derived
34
35 422 EIT system m is significantly smaller than the original one, so is the lin-
36
37 423 earised problem. Hence, by definition, this is a lower dimension problem so
38
39 424 intuitively should be a much faster problem to solve.

40
41 425 The advantages of the proposed scheme become more apparent as more
42
43 426 electrodes are engaged in the stimulation process. For clarity, the number
44
45 427 of electrode rings is increased to 4 and the corresponding singular spectrum
46
47 428 for the 4-ring electrode case is illustrated in Figure 4. As anticipated, a
48
49 429 significant gain improvement when compared with **Gain 2** is recorded and
50
51 430 the results are tabulated in Table 4 (**Gain 4**).

52
53 431 In the next section, the multiple-electrode pair scheme is applied to a
54
55 432 breast phantom.

5. Breast screening with EIT

It is evident from the previous sections that an increased number of electrodes is not necessarily a computational bottleneck. We refrain from discussing methods of accurately extracting the boundary shape of the breast or the technicalities of applying a large number of electrodes to the female breast skin as these topics are beyond the scope of this contribution. Rather, we refer to [21] for accurately extracting boundary surfaces.

Having demonstrated the effectiveness of the proposed scheme, the next sensible task is to report on the performance on a non-identity prior. For this purpose we employ the so called NOSER prior, which is essentially the diagonal of $\mathbf{J}^T \mathbf{J}$. We fix the number of electrodes to $L = 36$ and we illustrate a relatively fine (near the electrodes) mesh of a breast phantom in Figure 6 (top).

The performance of the original stimulation pattern ($L/d = 1$) is illustrated in Figure 5a) and the corresponding gains are tabulated in Table 5. As anticipated, the recorded gain (0.15364) is not far from the one recorded in **Gain 1**, $L = 36$, for the identity prior, i.e., 0.13281, **Gain 5**. However, an increase in the gain measure is reported when, as expected, the more efficient NOSER prior is used (**Gain 6**) for the same case ($L/d = 1$). Next, we test the proposed configuration for $L/d = 2$ electrodes per group against the conventional ($L/d = 1$) one. This action essentially supports the theme of this paper which is swap the single electrode groups for more electrode per group.

In Table 5 one may appreciate the performance of the suggested scheme for the priors considered herein. Clearly, increasing the number of electrodes

1
2
3
4
5
6
7
8
9
10 458 per firing-group results in a more efficient systems. This could be further
11 459 enhanced by the selection of the NOSER prior.

12
13 460 In summary, by suitably ‘clocking’ an EIT system with an appropriate
14
15 461 stimulation pattern as well as an appropriate prior, the performance of the
16
17 462 same system could be drastically improved from 0.15364 (**Gain 5**) to 0.9773
18
19 463 (**Gain 6**), not to mention data acquisition and computational times. If more
20
21 464 electrodes are considered, say $L = 48$, rather than 2112 measurements, only
22
23 465 180 measurements need to be collected. This accounts for approximately
24
25 466 8.52% of the original measurement number or a saving in the data acquisi-
26
27 467 tion time of approximately 91.48%. Thus, for this example, one could not
28
29 468 only derive a faster system but could also getaway with a fraction of the
30
31 469 conventional measurements.

32 470 In order to demonstrate that essentially no compromise in quality of the
33
34 471 reconstructed images is reported, we provide some representative reconstruc-
35
36 472 tion results. The question of the optimum regularisation value is essentially
37
38 473 an active research area where various methods could be used [29]. This is
39
40 474 beyond the scope of this paper as the answer lies with the problem at hand
41
42 475 and the specifications to be met. Therefore, images are reconstructed for
43
44 476 various equidistant logarithmic values for λ , ranging from $1e-1$ to $1e-8$, i.e.,
45
46 477 $\lambda = \{1.00000e-001, 1.33352e-002, 1.77828e-003, 2.37137e-004, 3.16228e-005,$
47
48 478 $4.21697e-006, 5.62341e-007, 7.49894e-008, 1.00000e-008\}$.

49 479 For clarity, we present linear reconstructions for the various configurations
50
51 480 reflecting the number of electrodes per firing-group, i.e., the conventional one
52
53 481 $L/d = 1$ -electrode per group in Figure 7, the proposed one for $L/d = 2$ -
54
55 482 electrode per group in Figure 8 and for $L/d = 6$ -electrode per group in

1
2
3
4
5
6
7
8
9
10 483 Figure 9. In each Figure, one depicts from the first column 2D coronal
11 484 slices extracted from the original 3D simulated perturbation. Essentially, we
12
13 485 extract 2D reconstructions at levels $\mathbf{h} = [-0.8, -0.6, -0.4, -0.2]^T$, hence 4
14
15 486 images per column. The columns next to the original 3D perturbation, i.e.,
16
17 487 columns 2-10 in each Figure, are reconstructions for the various values of λ .

18
19 488 To avoid biased reconstructions and essentially an inverse crime, mea-
20
21 489 surements and reconstructions were computed on different meshes. In effect,
22
23 490 measurements were collected from the fine mesh for a 10% perturbation, pre-
24
25 491 sented in Figure 6 (middle). As mentioned before, 25dB noise was added to
26
27 492 the measurements. All reconstructions were performed on a coarser mesh,
28
29 493 shown in Figure 6 (bottom). Herein, for all simulations the EIDORS toolbox
30
31 494 was employed [26].

33 495 **6. Discussion**

34
35
36 496 In our view, since EIT is an inverse problem, one should couple proposed
37
38 497 stimulation and measurement strategies with prior information. Further, as
39
40 498 it is clearly demonstrated by our numerical results, the 1-electrode group,
41
42 499 simply put, performs poorly. The advantages of the compound-electrode
43
44 500 pair outperform the conventional stimulation methods.

45
46 501 It would be of great interest to verify our numerical findings with realistic
47
48 502 measurements. The current bottleneck however, is that most available EIT
49
50 503 systems are configured (hardware-wise) to fire on single-electrode groups and
51
52 504 are typically manufactured with a little number of electrodes. As such, as
53
54 505 long as a multiple-electrode pair system becomes available to our disposal
55
56 506 we will publish our findings. Although that we have no mathematical means

1
2
3
4
5
6
7
8
9
10 507 to support such a statement at this stage, it appears that a ‘more random’
11 508 choice of non-opposite groups would probably increase the incoherence of \mathbf{J}
12
13 509 and would probably improve reconstruction quality.

14
15 510 On the other hand, by using the GSVD analysis, one could essentially pro-
16
17 511 vide a good indication of the amount of information that a specific coupling
18 512 (\mathbf{J}, \mathbf{R}) could offer to the inverse problem, before actually solving Equation
19
20 513 (13). In this light, it is of little surprise that the identity prior offered very
21
22 514 little improvement in the performance of the system. Indeed, the poor perfor-
23
24 515 mance indicated that major amendments in the selection of the regularisation
25
26 516 matrix were necessitated.

27 28 29 517 *6.1. Further work*

30
31 518 This study is part of our long term goal to derive model reduction schemes
32
33 519 in EIT without compromising on robustness and/or quality of acquired EIT
34
35 520 data/images. In this regard, a reduction in m was achieved and essentially
36
37 521 reflected in \mathbf{J} .

38
39 522 In [15], the author proposed multi-level basis functions (wavelets) as ba-
40
41 523 sis functions for both the forward and inverse computations of the soft-field
42
43 524 imaging problem in order to reduce dimensionality of \mathbf{J} (by compression).
44
45 525 This automatically enabled the ‘multi-level Jacobian’ and hence the multi-
46
47 526 level version of the forward version at no additional computational cost. To
48
49 527 the best of our knowledge such a configuration was not available before. It
50
51 528 is sensible therefore, to join the ideas developed in this article with the ideas
52
53 529 developed in [15] in order to offer a ‘possibly primitive’ model reduction
54
55 530 scheme that makes use of no additional transformation aside from the ones
56
57 531 required for the solution of the inverse problem. Needless to say that if ap-

1
2
3
4
5
6
7
8
9
10
11
12
13
14
15
16
17
18
19
20
21
22
23
24
25
26
27
28
29
30
31
32
33
34
35
36
37
38
39
40
41
42
43
44
45
46
47
48
49
50
51
52
53
54
55
56
57
58
59
60
61
62
63
64
65

532 appropriate, this could be further combined with other generic model reduction
533 methods, e.g., statistical ones [33], to offer additional significant advantages
534 in reconstruction timings.

535 On the other hand, there is no restriction on the use of non-linear schemes
536 to perform the reconstruction task. In fact, the proposed method, appears
537 to best suit non-linear systems where linearised steps are essential. Thus,
538 the proposed method has the potential to enable additional computational
539 savings. Not to mention that although real admittivities were considered
540 herein, there is no obvious limitation for the complex case. In this manner,
541 higher frequency model or multi-frequency EIT system could also be studied.

542 **7. Conclusion**

543 In this article, we numerically demonstrated that by engaging more than
544 one electrodes in the stimulation pattern, significant computational savings
545 could be reported. Moreover, it was shown that unlike conventional systems,
546 in the proposed configuration, as the number of electrodes increases so does
547 the performance of the proposed system. Simulations on simple tanks with
548 various numbers of electrode rings and number of electrodes per ring were
549 presented. Ideas developed were then applied to a breast phantom. Repre-
550 sentative reconstructions for the breast phantom were provided to emphasise
551 that despite the reduction in the number of collected measurements, no com-
552 promise in the quality of the reconstructed images is reported.

1
2
3
4
5
6
7
8
9
10 553 **Acknowledgements**

11
12 554 This work was supported by the Engineering and Physical Sciences Re-
13
14 555 search Council (EPSRC) under Grant EP/G061580/1.

15
16
17 556 **References**

- 18
19
20 557 [1] WHO, World Health Organisation, [http://www.who.int/mediacentre/](http://www.who.int/mediacentre/factsheets/fs297/en/)
21
22 558 [factsheets/fs297/en/](http://www.who.int/mediacentre/factsheets/fs297/en/) N297.
- 23
24 559 [2] BCCUK, Breast cancer care UK, [http://www.breastcancercare.org.uk/](http://www.breastcancercare.org.uk/news/media-centre/facts-statistics)
25
26 560 [news/media-centre/facts-statistics](http://www.breastcancercare.org.uk/news/media-centre/facts-statistics).
- 27
28
29 561 [3] C. W. Piccoli, Contrast-enhanced breast mri: factors affecting sensitiv-
30
31 562 ity and specificity., *European Radiology* 7 Suppl 5 (1997) 281–288.
- 32
33
34 563 [4] P. T. Huynh, A. M. Jarolimek, S. Daye, The false-negative mammo-
35
36 564 gram., *Radiographics* 18 (5) (1998) 1137–1154.
- 37
38
39 565 [5] P. H. Kuo, E. Kanal, A. K. Abu-Alfa, S. E. Cowper, Gadolinium-
40
41 566 based MR contrast agents and nephrogenic systemic fibrosis1, *Radiology*
42
43 567 242 (3) (2007) 647–649.
- 44
45 568 [6] M. S. Bae, W. Han, H. R. Koo, N. Cho, J. M. Chang, A. Yi, I.-A. Park,
46
47 569 D.-Y. Noh, W. S. Choi, W. K. Moon, Characteristics of breast cancers
48
49 570 detected by ultrasound screening in women with negative mammograms,
50
51 571 *Cancer Science* 102 (10) (2011) 1862–1867.
- 52
53
54 572 [7] M. Soleimani, R. H. Bayford, New and emerging tomographic imaging
55
56 573 techniques in medical and industrial applications, *Philosophical Trans-*

1
2
3
4
5
6
7
8
9
10
11
12
13
14
15
16
17
18
19
20
21
22
23
24
25
26
27
28
29
30
31
32
33
34
35
36
37
38
39
40
41
42
43
44
45
46
47
48
49
50
51
52
53
54
55
56
57
58
59
60
61
62
63
64
65

574 actions of the Royal Society A: Mathematical, Physical and Engineering
575 Sciences 367 (1900) (2009) 3017–3019.

576 [8] Draeger, Pulmovista 500®, <http://www.draeger.com/>.

577 [9] M. Lazebnik, D. Popovic, L. McCartney, C. B. Watkins, M. J. Lind-
578 strom, J. Harter, S. Sewall, T. Ogilvie, A. Magliocco, T. M. Breslin,
579 W. Temple, D. Mew, J. H. Booske, M. Okoniewski, S. C. Hagness, A
580 large-scale study of the ultrawideband microwave dielectric properties
581 of normal, benign and malignant breast tissues obtained from cancer
582 surgeries, *Physics in Medicine and Biology* 52 (20) (2007) 6093.

583 [10] M. Assenheimer, O. Laver-Moskovitz, D. Malonek, D. Manor, U. Na-
584 haliel, R. Nitzan, A. Saad, The t-scan technology: electrical impedance
585 as a diagnostic tool for breast cancer detection., *Physiological Measure-*
586 *ment* 22 (1) (2001) 1–8.

587 [11] N. Polydorides, Image reconstruction algorithms for soft-field tomogra-
588 phy, Ph.D. thesis, UMIST, UK (2002).

589 [12] A. Borsic, Regularisation methods for imaging from electrical measure-
590 ments, Ph.D. thesis, Oxford Brookes University, UK (2002).

591 [13] M. Soleimani, Image and shape reconstruction in Magnetic induc-
592 tion and Electrical Impedance Tomography, Ph.D. thesis, University
593 of Manchester (2005).

594 [14] T. Dai, Image reconstruction in EIT using advanced regularization
595 frameworks, Ph.D. thesis, Carleton University, Canada (2008).

- 1
2
3
4
5
6
7
8
9
10 596 [15] P. Kantartzis, Multilevel soft-field tomography, Ph.D. thesis, City Uni-
11 597 versity London, UK (2011).
- 12
13
14 598 [16] M. Cheney, D. Isaacson, Distinguishability in impedance imaging,
15
16 599 Biomedical Engineering, IEEE Transactions on 39 (8) (1992) 852 –860.
- 17
18
19 600 [17] W. R. B. Lionheart, J. Kaipio, C. N. McLeod, Generalized optimal
20
21 601 current patterns and electrical safety in EIT, Physiological Measurement
22
23 602 22 (1) (2001) 85.
- 24
25 603 [18] A. Adler, P. O. Gaggero, Y. Maimaitijiang, Adjacent stimulation and
26
27 604 measurement patterns considered harmful, Physiological Measurement
28
29 605 32 (7) (2011) 731.
- 30
31
32 606 [19] A. Adler, R. Youmaran, W. R. B. Lionheart, A measure of the infor-
33
34 607 mation content of EIT data, Physiological Measurement 29 (6) (2008)
35
36 608 S101.
- 37
38
39 609 [20] A. Boyle, A. Adler, The impact of electrode area, contact impedance
40
41 610 and boundary shape on EIT images, Physiological Measurement 32 (7)
42
43 611 (2011) 745.
- 44
45 612 [21] J. Forsyth, A. Borsic, R. J. Halter, A. Hartov, K. D. Paulsen, Optical
46
47 613 breast shape capture and finite-element mesh generation for Electrical
48
49 614 Impedance Tomography, Physiological Measurement 32 (7) (2011) 797.
- 50
51
52 615 [22] H. Dehghani, N. Soni, R. Halter, A. Hartov, K. D. Paulsen, Excita-
53
54 616 tion patterns in three-dimensional Electrical Impedance Tomography,
55
56 617 Physiological Measurement 26 (2) (2005) S185.

- 1
2
3
4
5
6
7
8
9
10 618 [23] N. Polydorides, H. McCann, Electrode configurations for improved spa-
11 619 tial resolution in Electrical Impedance Tomography, Measurement Sci-
12 620 ence and Technology 13 (12) (2002) 1862.
- 13
14
15
16 621 [24] N. Soni, K. Paulsen, H. Dehghani, A. Hartov, Finite element imple-
17 622 mentation of maxwell's equations for image reconstruction in electrical
18 623 impedance tomography, Medical Imaging, IEEE Transactions on 25 (1)
19 624 (2006) 55 –61.
- 20
21
22
23
24 625 [25] N. Polydorides, W. R. B. Lionheart, A matlab toolkit for three-
25 626 dimensional electrical impedance tomography: a contribution to the
26 627 electrical impedance and diffuse optical reconstruction software project,
27 628 Meas. Sc. Tech. 13 (12) (2002) 1871–1883.
- 28
29
30
31
32
33 629 [26] EIDORS, Electrical impedance tomography and diffuse optical tomog-
34 630 raphy reconstruction software, <http://eidors3d.sourceforge.net/>.
- 35
36
37 631 [27] N. Polydorides, W. R. B. Lionheart, Adjoint formulations in impedance
38 632 imaging, Proc. 3rd Cong. Indust. Proc. Tomog.
- 39
40
41
42 633 [28] E. Somersalo, M. Cheney, D. Isaacson, Existence and uniqueness for
43 634 electrode models for electric-current-computed tomography, SIAM J.
44 635 App. Math. 52 (4) (1992) 1023–1040.
- 45
46
47
48
49 636 [29] P. C. Hansen, Rank deficient and discrete ill-posed problems, SIAM,
50 637 Philadelphia, PA, USA, 1998.
- 51
52
53 638 [30] O. Scherzer, Handbook of Mathematical Methods in Imaging, 1st Edi-
54 639 tion, Springer-Verlag, 2010.
- 55
56
57
58
59
60
61
62
63
64
65

1
2
3
4
5
6
7
8
9
10
11
12
13
14
15
16
17
18
19
20
21
22
23
24
25
26
27
28
29
30
31
32
33
34
35
36
37
38
39
40
41
42
43
44
45
46
47
48
49
50
51
52
53
54
55
56
57
58
59
60
61
62
63
64
65

640 [31] G. H. Golub, C. F. Van Loan, Matrix Computations, 2nd Edition, Johns
641 Hopkins Press, Baltimore, MD, 1989.

642 [32] J. Schorberl, Netgen - an Advancing front 2d/3d mesh generator based
643 on abstract rules, Computing and Visualization in Science 1 (1) (1997)
644 41–52.

645 [33] A. Nissinen, L. M. Heikkinen, J. P. Kaipio, The bayesian approximation
646 error approach for electrical impedance tomographyexperimental results,
647 Measurement Science and Technology 19 (1) (2008) 015501.

1
2
3
4
5
6
7
8
9
10
11
12
13
14
15
16
17
18
19
20
21
22
23
24
25
26
27
28
29
30
31
32
33
34
35
36
37
38
39
40
41
42
43
44
45
46
47
48
49
50
51
52
53
54
55
56
57
58
59
60
61
62
63
64
65

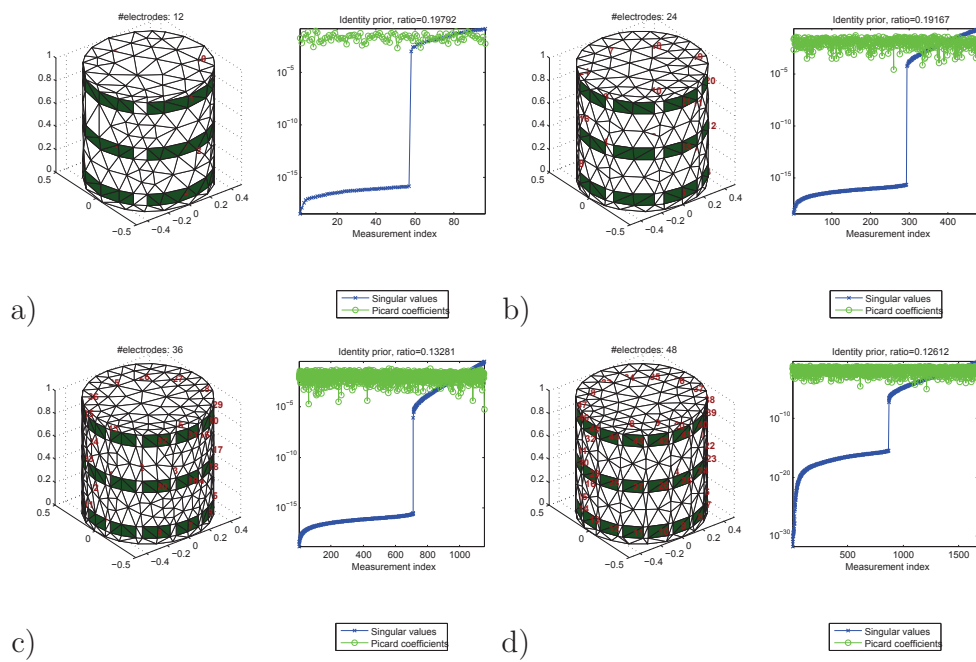


Figure 1: Conventional opposite 2-electrode pair stimulation protocol: Picard's coefficients superimposed to the generalised singular values for a cylindrical tank test phantom where 3 rings of electrodes are attached. The total number of electrodes is a) 12, b) 24, c) 36 and d) 48.

1
2
3
4
5
6
7
8
9
10
11
12
13
14
15
16
17
18
19
20
21
22
23
24
25
26
27
28
29
30
31
32
33
34
35
36
37
38
39
40
41
42
43
44
45
46
47
48
49
50
51
52
53
54
55
56
57
58
59
60
61
62
63
64
65

Electrodes L	Measurements m	L/m	Gain 1
12	96	0.12500	0.19792
24	480	0.05000	0.19167
36	1152	0.03125	0.13281
48	2112	0.02273	0.12612

Table 1: Conventional opposite 2-electrode pair stimulation protocol gains: **Gain** is the ratio of the practically available generalised singular values against the total number of generalised singular values for a cylindrical tank test phantom where 3 rings of electrodes are allowed.

1
2
3
4
5
6
7
8
9
10
11
12
13
14
15
16
17
18
19
20
21
22
23
24
25
26
27
28
29
30
31
32
33
34
35
36
37
38
39
40
41
42
43
44
45
46
47
48
49
50
51
52
53
54
55
56
57
58
59
60
61
62
63
64
65

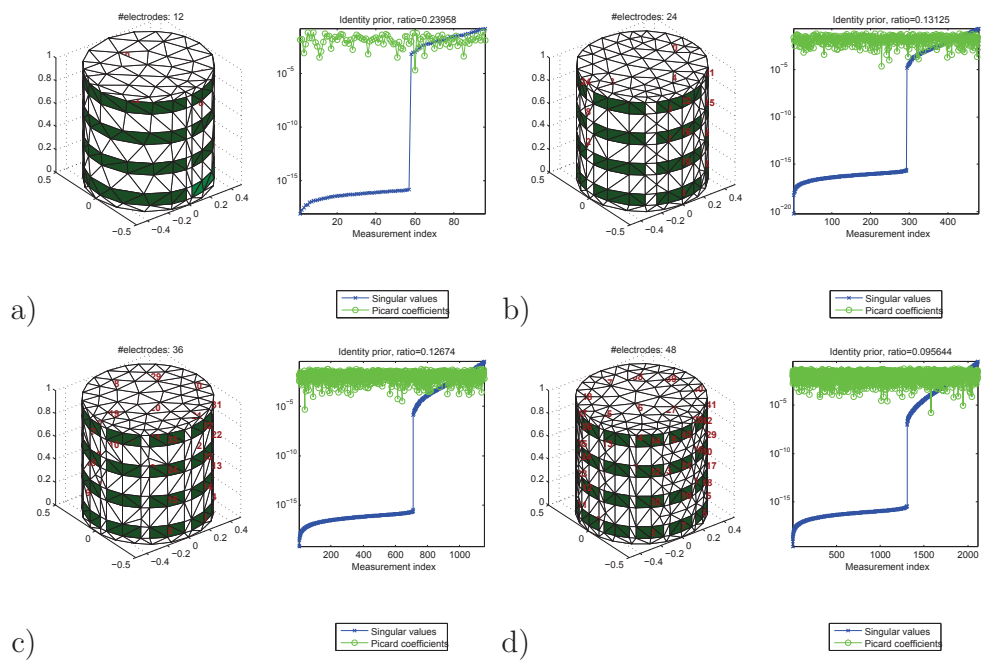


Figure 2: Conventional opposite 2-electrode pair stimulation protocol: Picard's coefficients superimposed to the generalised singular values for a cylindrical tank test phantom where 4 rings of electrodes are attached. The total number of electrodes is a) 12, b) 24, c) 36 and d) 48.

1
2
3
4
5
6
7
8
9
10
11
12
13
14
15
16
17
18
19
20
21
22
23
24
25
26
27
28
29
30
31
32
33
34
35
36
37
38
39
40
41
42
43
44
45
46
47
48
49
50
51
52
53
54
55
56
57
58
59
60
61
62
63
64
65

Electrodes L	Measurements m	L/m	Gain 2
12	96	0.12500	0.23958
24	480	0.05000	0.13125
36	1152	0.03125	0.12674
48	2112	0.02273	0.09564

Table 2: Conventional opposite 2-electrode pair stimulation protocol gains: **Gain** is the ratio of the practically available generalised singular values against the total number of generalised singular values for a cylindrical tank test phantom where 4 rings of electrodes are allowed.

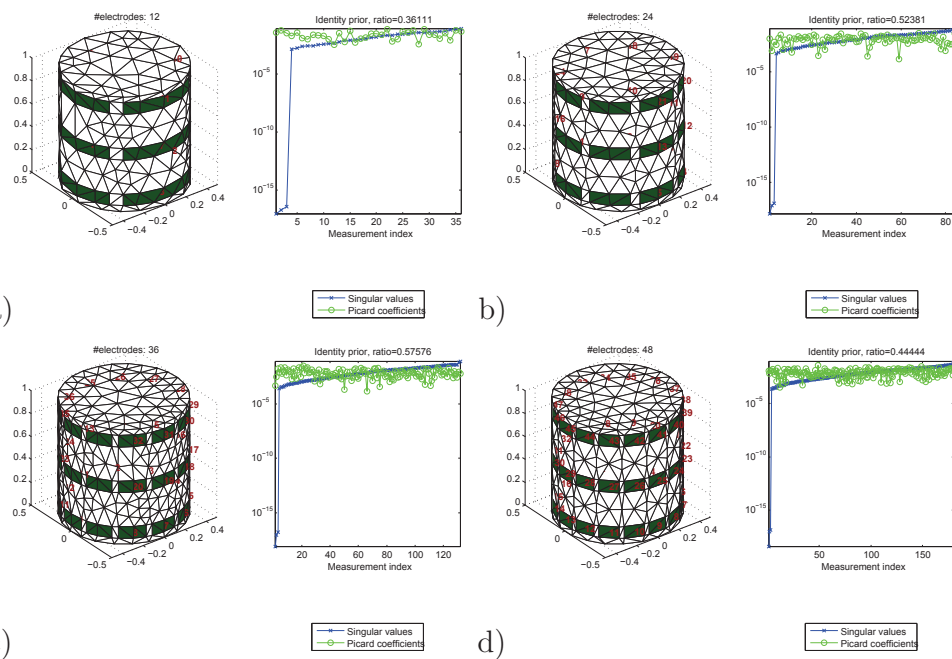


Figure 3: Proposed opposite protocol ($d = 6$ driving patterns): Picard's coefficients superimposed to the generalised singular values for a cylindrical tank test phantom where 3 rings of electrodes are attached. The total number of electrodes is a) 12, b) 24, c) 36 and d) 48.

1
2
3
4
5
6
7
8
9
10
11
12
13
14
15
16
17
18
19
20
21
22
23
24
25
26
27
28
29
30
31
32
33
34
35
36
37
38
39
40
41
42
43
44
45
46
47
48
49
50
51
52
53
54
55
56
57
58
59
60
61
62
63
64
65

Electrodes L	Measurements m	L/m	Gain $\mathbf{3}$
12	36	0.333333	0.361111
24	84	0.285714	0.523810
36	132	0.272727	0.575758
48	180	0.266667	0.444444

Table 3: Proposed opposite protocol gains ($d = 6$ driving patterns): **Gain 3** is the ratio of the practically available generalised singular values against the total number of generalised singular values for a cylindrical tank test phantom where 3 rings of electrodes are allowed.

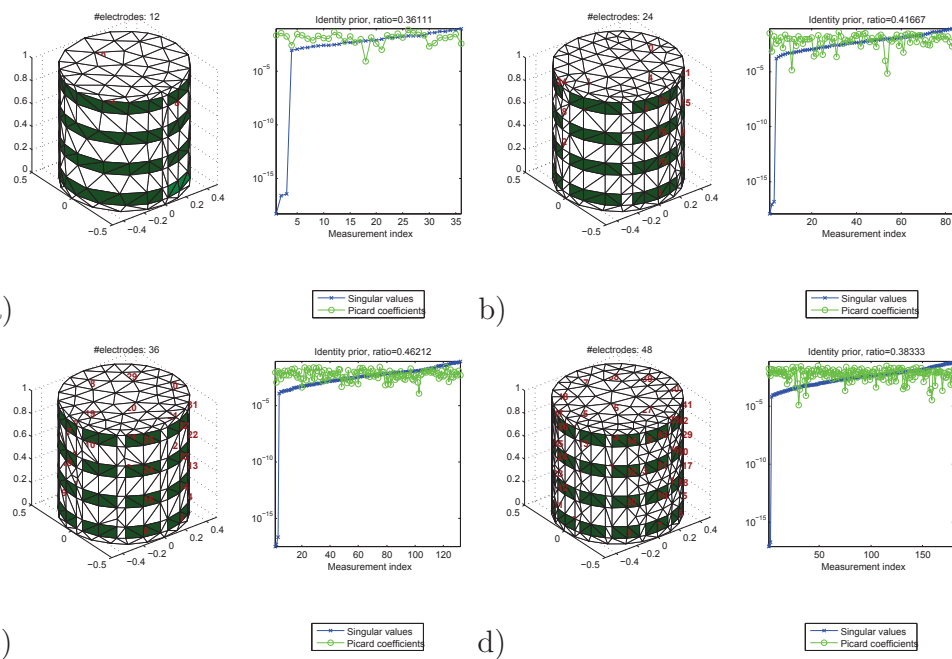


Figure 4: Proposed opposite protocol ($d = 6$ driving patterns): Picard's coefficients superimposed to the generalised singular values for a cylindrical tank test phantom where 4 rings of electrodes are attached. The total number of electrodes is a) 12, b) 24, c) 36 and d) 48.

1
2
3
4
5
6
7
8
9
10
11
12
13
14
15
16
17
18
19
20
21
22
23
24
25
26
27
28
29
30
31
32
33
34
35
36
37
38
39
40
41
42
43
44
45
46
47
48
49
50
51
52
53
54
55
56
57
58
59
60
61
62
63
64
65

Electrodes L	Measurements m	L/m	Gain 4
12	36	0.33333	0.36111
24	84	0.28571	0.41667
36	132	0.27273	0.46212
48	180	0.26667	0.38333

Table 4: Proposed opposite protocol gains ($d = 6$ driving patterns): **Gain 4** is the ratio of the practically available generalised singular values against the total number of generalised singular values for a cylindrical tank test phantom where 4 rings of electrodes are allowed.

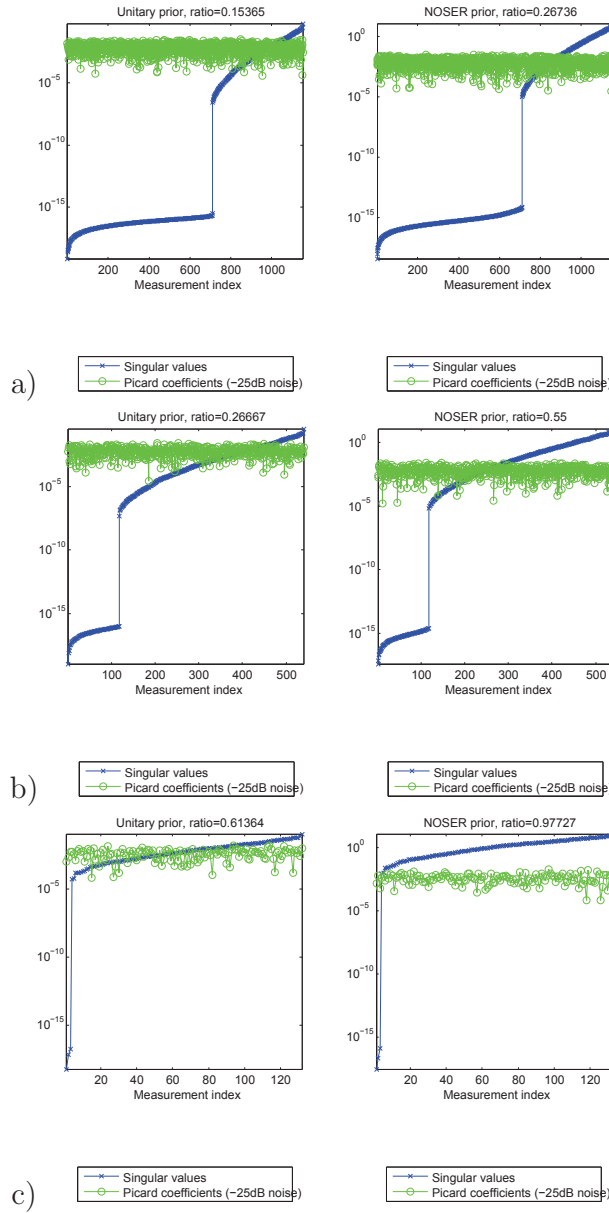


Figure 5: Conventional versus proposed opposite protocol for various numbers L/d of electrodes per stimulation group. a) $L/d = 1$, b) $L/d = 2$ and c) $L/d = 6$ electrodes per groups. In the left column results shown assume a simple identity prior and in the right column results shown assume the NOSER prior.

1
2
3
4
5
6
7
8
9
10
11
12
13
14
15
16
17
18
19
20
21
22
23
24
25
26
27
28
29
30
31
32
33
34
35
36
37
38
39
40
41
42
43
44
45
46
47
48
49
50
51
52
53
54
55
56
57
58
59
60
61
62
63
64
65

L/d	Electrodes L	Measurements m	L/m	Gain 5	Gain 6
1	36	1152	0.03125	0.15364	0.26736
2	36	540	0.06671	0.26673	0.55001
6	36	132	0.27274	0.61361	0.97731

Table 5: Comparison between conventional ($L/d = 1$) and proposed ($L/d = 2, 6$) opposite protocol gains for the breast phantom. Priors considered herein are the Identity (**Gain 5**) and the NOSER (**Gain 6**) one.

1
2
3
4
5
6
7
8
9
10
11
12
13
14
15
16
17
18
19
20
21
22
23
24
25
26
27
28
29
30
31
32
33
34
35
36
37
38
39
40
41
42
43
44
45
46
47
48
49
50
51
52
53
54
55
56
57
58
59
60
61
62
63
64
65

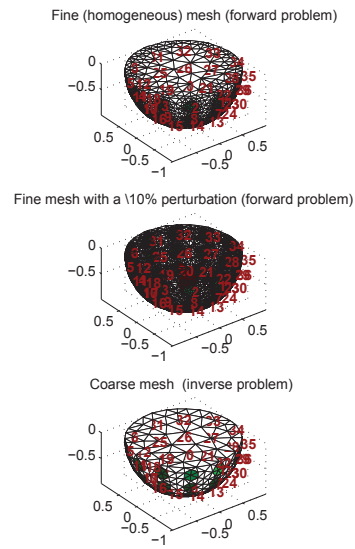


Figure 6: Breast phantom meshes: (Top, middle) Fine meshes used to simulate measurements. In the middle a 10%, 3D perturbation is shown. (bottom) A coarser mesh to be used for reconstruction purposes.

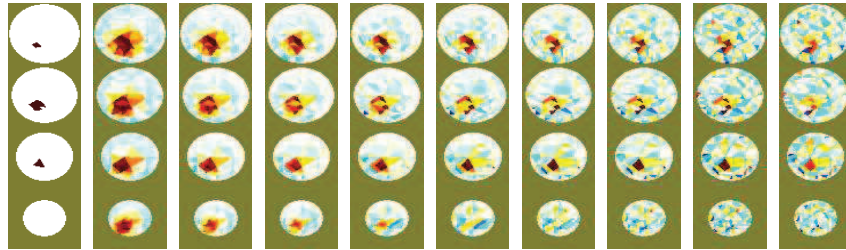


Figure 7: Conventional opposite protocol ($L/d = 1$ electrodes per group). First column is the original 3D perturbation presented as 2D coronal slices of the breast phantom at levels \mathbf{h} . Remaining columns (2-10) are reconstructions for various values of the regularisation parameter $\lambda = \{1.00000\text{e-}001, 1.33352\text{e-}002, 1.77828\text{e-}003, 2.37137\text{e-}004, 3.16228\text{e-}005, 4.21697\text{e-}006, 5.62341\text{e-}007, 7.49894\text{e-}008, 1.00000\text{e-}008\}$.

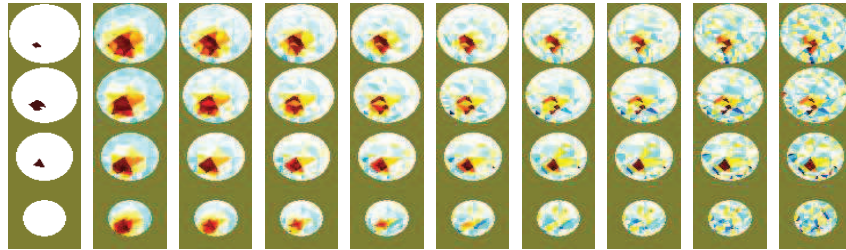


Figure 8: Proposed opposite protocol ($L/d = 2$ electrodes per group). First column is the original 3D perturbation presented as 2D coronal slices of the breast phantom at levels **h**. Remaining columns (2-10) are reconstructions for various values of the regularisation parameter $\lambda = \{1.00000e-001, 1.33352e-002, 1.77828e-003, 2.37137e-004, 3.16228e-005, 4.21697e-006, 5.62341e-007, 7.49894e-008, 1.00000e-008\}$.

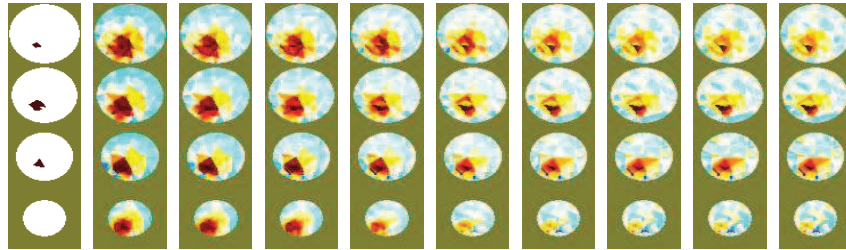


Figure 9: Proposed opposite protocol ($L/d = 6$ electrodes per group). First column is the original 3D perturbation presented as 2D coronal slices of the breast phantom at levels **h**. Remaining columns (2-10) are reconstructions for various values of the regularisation parameter $\lambda = \{1.00000e-001, 1.33352e-002, 1.77828e-003, 2.37137e-004, 3.16228e-005, 4.21697e-006, 5.62341e-007, 7.49894e-008, 1.00000e-008\}$.

Highlights:

- Improved stimulation protocol for 3D impedance imaging;
- Suitable for excessive electrodes in 3D geometries, e.g., breast imaging;
- Reduction in number of measurements and data acquisition timings;
- Improved performance for the same impedance imaging system;
- No compromise on the quality of reconstructed images;